# X-ray Structure and Physical Properties of the Oxo-Bridged Complex [($F_8$-TPP)Fe-O-Cu(TMPA)]$^+$, $F_8$-TPP = Tetrakis(2,6-difluorophenyl)porphyrinate(2–), TMPA = Tris(2-pyridylmethyl)amine: Modeling the Cytochrome *c* Oxidase Fe–Cu Heterodinuclear Active Site

**Kenneth D. Karlin,*,† Alaganandan Nanthakumar,† Stephen Fox,† Narasimha N. Murthy,† Natarajan Ravi,‡ Boi Hanh Huynh,*,‡ Robert D. Orosz,‡ and Edmund P. Day*,‡**

*Contribution from the Department of Chemistry, The Johns Hopkins University, Charles & 34th Streets, Baltimore, Maryland 21218, and Department of Physics, Emory University, 1510 Clifton Road NE, Atlanta, Georgia 30322*

*Received November 23, 1993*®

**Abstract:** The iron/copper heterodinuclear center in cytochrome *c* oxidases has attracted the interest of inorganic chemists since this is the site of dioxygen ($O_2$) four-electron four-proton reduction to water by the reduced enzyme, while the oxidized ("resting") isolated protein dinuclear center exhibits unusual physical, spectroscopic, and ligand-binding properties. We describe here a model compound, [($F_8$-TPP)$Fe^{III}$-O-$Cu^{II}$(TMPA)]$^+$ (**3**), generated directly from $O_2$-reduction by 1:1 mixtures of the reduced copper(I) and iron(II) complexes [(TMPA)$Cu^I(CH_3CN)]^+$ (**1**) (TMPA = tris(2-pyridylmethyl)amine) and ($F_8$-TPP)$Fe^{II}(pip)_2$ (**2**) ($F_8$-TPP = tetrakis(2,6-difluorophenyl)porpyrinate-(2–), pip = piperidine) in $O_2$-saturated $CH_2Cl_2$ at –80 °C; warming to 0 °C, followed by precipitation with diethyl ether, affords **3** in ~70% yield. An X-ray diffraction study on [($F_8$-TPP)Fe-O-Cu(TMPA)]$(ClO_4)\cdot 3C_7H_8\cdot 2CH_3CN$ (**3**-$ClO_4$) as well as the μ-oxo iron dimer [($F_8$-TPP)Fe]$_2O\cdot 3C_7H_8$ allows for direct structural comparisons, as well as with other relevant compounds. Compound **3** also possesses a linear μ-oxo-bridging ligand, where ∠Fe–O–Cu = 178.2-(4)°; unusually short metal–oxygen distances of Fe–O = 1.740(5) Å and Cu–O = 1.856(5) Å are observed, and Fe···Cu = 3.596(2) Å. The coordination geometry around Cu is distorted from the usual (i.e., for TMPA–Cu(II) complexes) trigonal-bipyramidal configuration toward a square-based pyramidal arrangement, and the three pyridine rings are situated between the four $F_8$-TPP phenyl rings, thus leaving one "slot" free. $^1$H-NMR spectra of **3**-$ClO_4$ in $CD_2Cl_2$ exhibit a pyrrole signal at 65 ppm (corroborated by $^2$H-NMR) which is upfield shifted relative to other axially symmetric high-spin (tetraphenylporphyrinate)iron(III) complexes; this is consistent with electronic/magnetic coupling of the Fe(III) and Cu(II) centers. Additional upfield-shifted signals are tentatively assigned to the TMPA ligand on copper, thus implicating a bridged structural arrangement which is maintained in solution. A detailed magnetic Mössbauer spectroscopic study (4.2 K at 0, 0.5, and 8 T) has been carried out. The data unambiguously indicate that **3** possesses a high-spin ferric ($S_{Fe}$ = 5/2) ion and exhibits characteristic parameters: $D = 6.0 \pm 0.5$ cm$^{-1}$, $E/D = 0.03 \pm 0.01$, $\Delta E_Q = -1.26 \pm 0.02$ mm/s, $\eta = 0$, $\delta = 0.46 \pm 0.01$ mm/s, and $A/g_n\beta_n = -23.7 \pm 0.3$ T. Furthermore, the magnetic properties observed, i.e., in the presence or absence of an applied field, demonstrate that the ferric ion is spin-coupled to the cupric ion to form an overall integer spin system in [($F_8$-TPP)$Fe^{III}$-O-$Cu^{II}$(TMPA)]$(ClO_4)$ (**3**-$ClO_4$). The Mössbauer isomer shift and quadrupole splitting parameters compare favorably with those previously obtained for data on enzyme resting-state preparations, although they differ in certain details. The conclusion that **3**-$ClO_4$ is an $S$ = 2 system is determined by multifield saturation magnetization measurements, carried out both in solution (2–200 K) and the solid state (30–300 K). An exact magnetic coupling constant $J$ (for exchange coupling according to $(-2J\mathbf{S}_1\cdot\mathbf{S}_2)$) could not be determined from the solution data, due to the inherent "noise" found in these measurements, even for ~1 mM solutions. These findings call into question previous evaluations for the lower limit of $|J| \geq 200$ cm$^{-1}$ for the dinuclear Fe(III)-X-Cu(II) site in as-isolated "resting" oxidized cytochrome *c* oxidase enzyme; a lower limit of $|J|$ greater than 50 cm$^{-1}$ is suggested as a better estimate. Solid-state measurements on **3**-$ClO_4$ give a value of $-J$ = 87 cm$^{-1}$, i.e., moderately strong antiferromagnetic coupling between high-spin iron(III) and copper(II) ions, consistent with the NMR and Mössbauer spectroscopic data. The possible biological relevance of the oxo-bridged complex [($F_8$-TPP)$Fe^{III}$-O-$Cu^{II}$(TMPA)]$ClO_4$) (**3**-$ClO_4$) and its observed magnetic/electronic properties are discussed.

## Introduction

Cytochrome *c* oxidases (C*c*O's) are membrane-bound metalloenzymes which catalyze the four-electron, four-proton reduction of dioxygen to water (eq 1).[1,2] This exergonic process is

$$O_2 + 4H^+ + 4e^- \text{ (from cyt } c) \rightarrow 2H_2O \qquad (1)$$

coupled to proton translocation across the membrane to generate a pH gradient and membrane potential, which is harnessed through the subsequent synthesis of ATP. Mammalian mito-

* To whom correspondence should be addressed.
† The Johns Hopkins University.
‡ Emory University.
® Abstract published in *Advance ACS Abstracts*, April 15, 1994.

(1) (a) Malmström, B. G. *Acc. Chem. Res.* **1993**, *26*, 332–338. (b) Fee, J. A.; Antholine, W. E.; Fan, C.; Gurbiel, R. J.; Surerus, K.; Werst, M.; Hoffman, B. M. In *Bioinorganic Chemistry of Copper*; Karlin, K. D., Tyeklár, Z., Eds.; Chapman & Hall: New York, 1993; pp 485–500. (c) Babcock, G. T.; Wikström, M. *Nature* **1992**, *356*, 301–309, and references cited therein. (d) Chan, S. I.; Li, P. M. *Biochemistry* **1990**, *29*, 1–12. (e) Scott, R. A. *Annu. Rev. Biophys. Biophys. Chem.* **1989**, *18*, 137–158.

(2) (a) Hosler, J. P.; Ferguson-Miller, S.; Calhoun, M. W.; Thomas, J. W.; Hill, J.; Lemieux, L.; Ma, J.; Georgiou, C.; Fetter, J.; Shapleigh, J.; Tecklenburg, M. M. J.; Babcock, G. T.; Gennis, R. B. *J. Bioenerg. Biomembr.* **1993**, *25* (2), 121–136. (b) A minireview series devoted to cytochrome oxidase appears in the following: *J. Bioenerg. Biomembr.* **1993**, *25* (2), 69–188.

0002-7863/94/1516-4753$04.50/0 

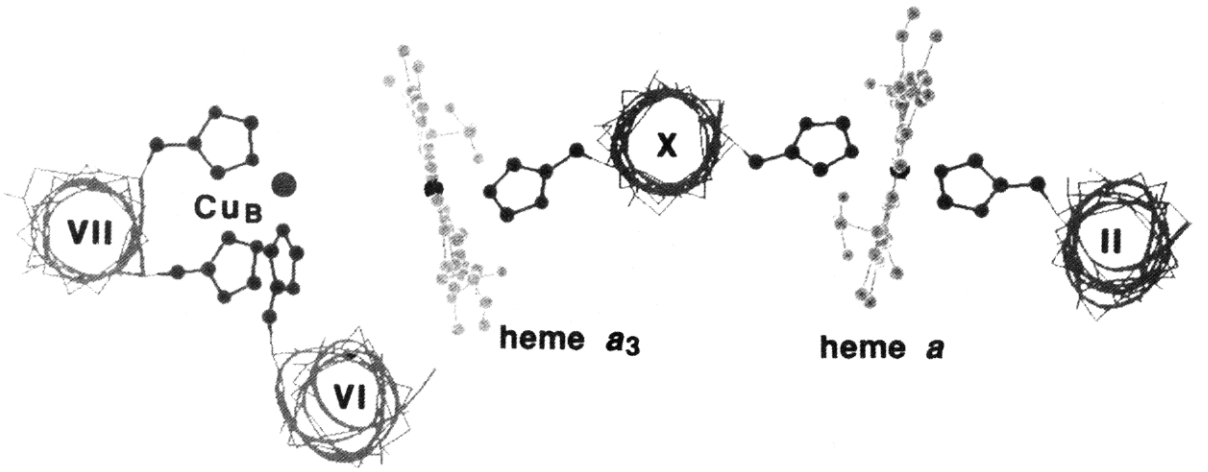


**Figure 1.** Current picture of the cytochrome oxidase arrangement of key transmembrane protein helices and deduced histidine ligation for the heme and copper site catalytic machinery responsible for dioxygen reduction. Other conserved residues are not shown (adapted from ref 2).

chondrial C*c*O has been extensively studied, but fresh insights have come from investigations on structurally simpler aerobic bacterial enzymes, containing fewer subunits, which are amenable to genetic manipulation, including site-directed mutagenesis studies.[2] Thus, a large variety of both eukariotic and prokariotic oxidases possess related structural features and most likely similar catalytic mechanisms for $O_2$-reduction. In $aa_3$-type C*c*O's, the electron flow appears to proceed from the cytochrome *c* substrate (i.e., electron donor) to the so-called $Cu_A$ site residing in subunit II;[1a,3] the latter center most likely consists of a dinuclear mixed-valent Cu(I)–Cu(II) center.[4] However, the structurally and functionally similar ubiquinol oxidases, $aa_3$ from *Bacillus subtilis* and related *bo*-type, lack $Cu_A$;[5] these enzymes utilize a quinol electron donor as substrate.[2] Thus, in the general case, electrons from the appropriate donor are passed to the catalytic "machinery" in subunit I, first to heme *a* (or *b*) and then to the dinuclear heme $a_3$-iron (or heme *o*) copper($Cu_B$) unit.[1a,3] A current biochemically inferred simplified representation of the subunit I active site arrangement of metal centers is given in Figure 1, also showing the key histidyl nitrogen donor ligands deduced to be present.[2]

The critical $O_2$-binding, reduction, and protonation steps relating to eq 1 occur at the dinuclear Fe/Cu heme $a_3$–$Cu_B$ site.[1,2] The enzyme is activated by reduction of the dinuclear center to the $Fe^{II}$ and $Cu^{I}$ oxidation states. Time-resolved kinetic–spectroscopic investigations have provided insights into the nature of the reaction and identity of intermediates, Scheme 1.[1a,6] Dioxygen initially interacts with $Cu_B^{I}$, producing a $Cu_B$–$O_2$ adduct[1a,7] and then switches ligation to give an Fe($a_3$)–$O_2$ species. There is some controversy concerning the exact sequence of subsequent events and vibrational assignments of the various species,[6] but production of an iron(III) peroxide or hydroperoxide intermediate occurs; whether $Cu_B$ ligation occurs is unclear. Cleavage of the O–O bond leads to a distinctive ferryl species (i.e., Fe(IV)=O), and further reduction and protonation complete the reaction.

**Scheme 1**

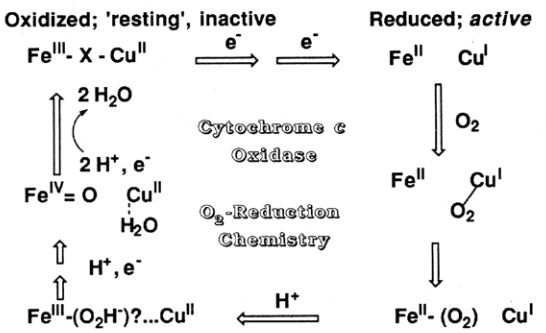


Final products such as $Fe^{III}$–OH and $Cu_B^{II}$–OH species have also been implicated, but the fully oxidized enzyme as usually purified and isolated contains an EPR silent, antiferromagnetically coupled $Fe^{III}$–X–$Cu_B^{II}$ moiety, where X has variously been suggested to be an oxo ($O^{2-}$), hydroxo, chloro, sulfido, cysteinato, or imidazolato group. Recent EXAFS (extended X-ray absorption fine structure) spectroscopic measurements on $aa_3$ from *B. subtilis* implicate a heavy-atom scatterer, suggested to be a chloride bridge;[8] one wonders, however, if $Cl^-$ could be exogenously derived during protein purification and manipulation. An active site conserved helix VI (Figure 1) glutamic acid residue has also recently been speculated to be this resting-state bridging ligand.[2a] The resting oxidized form has also been used in studies where the binding of ligands such as azide ($N_3^-$), cyanide ($CN^-$), or formate ($HCO_2^-$) results in the formation of $Fe_{a3}$–$Cu_B$ site adducts which are amenable to probing by techniques such as X-ray absorption,[1e] EPR, Mössbauer and infrared spectroscopies, or magnetic measurements.[1,2,9–11]

All the intermediates invoked above have separate precedent as coordination complexes, although none are in a dinuclear iron–

(3) Hill, B. C. *J. Bioenerg. Biomembr.* **1993**, *25* (2), 115–120.
(4) (a) Antholine, W. E.; Kastrau, D. H. W.; Steffens, G. C. M.; Buse, G.; Zumft, W. G.; Kroneck, P. M. H. *Eur. J. Biochem.* **1992**, *209*, 875–881. (b) Kelly, M.; Lappalainen, P.; Talbo, G.; Haltia, T.; van der Oost, J.; Saraste, M. *J. Biol. Chem.* **1993**, *268*, 16781–16787. (c) Palmer, G. *J. Bioenerg. Biomembr.* **1993**, *25* (2), 145–151.
(5) Lauraeus, M.; Haltia, T.; Saraste, M.; Wikström, M. *Eur. J. Biochem.* **1991**, *197*, 699.
(6) (a) Varotsis, C.; Zhang, Y.; Appelman, E. H.; Babcock, G. T. *Proc. Natl. Acad. Sci. U.S.A.* **1993**, *90*, 237–241. (b) Ogura, T.; Takahashi, S.; Hirota, S.; Shinzawa-Itoh, K.; Yoshikawa, S.; Appelman, E. H.; Kitagawa, T. *J. Am. Chem. Soc.* **1993**, *115*, 8527–8536.
(7) (a) Oliveberg, M.; Malmström, B. G. *Biochemistry* **1992**, *31*, 3560–3563. (b) Blackmore, R. S.; Greenwood, C.; Gibson, Q. H. *J. Biol. Chem.* **1991**, *266*, 19245–19249. (c) Woodruff, W. H.; Einarsdóttir, O.; Dyer, R. B.; Bagley, K. A.; Palmer, G.; Atherton, S. J.; Boldbeck, R. A.; Dawes, T. D.; Kliger, D. S. *Proc. Natl. Acad. Sci. U.S.A.* **1991**, *88*, 2588–2592.
(8) (a) Lauraeus, M.; Powers, L.; Chance, B.; Wikström, M. *J. Inorg. Biochem.* **1993**, *51*, 274. (b) George, G. N.; Cramer, S. P.; Frey, T. G.; Prince, R. C. *Biochim. Biophys. Acta* **1993**, *1142*, 240–252.
(9) Recent studies emphasizing probing $CN^-$, $SCN^-$, or $N_3^-$ by FT infrared spectroscopy: (a) Yoshikawa, S.; Caughey, W. S. *J. Biol. Chem.* **1992**, *267*, 9757–9766. (b) Li, W.; Palmer, G. *Biochemistry* **1993**, *32*, 1833–1843. (c) Tsubaki, M. *Biochemistry* **1993**, *32*, 174–182. See also published correction: *Biochemistry* **1993**, *32*, 9262. (d) Tsubaki, M.; Mogi, T.; Anraku, Y.; Hori, H. *Biochemistry* **1993**, *32*, 6065–6072.
(10) Studies of formate binding: (a) Watmough, N. J.; Cheesman, M. R.; Gennis, R. B.; Greenwood, C.; Thomson, A. J. *FEBS Lett.* **1993**, *319*, 151–154. (b) Ingledew, W. J.; Horrocks, J.; Salerno, J. C. *Eur. J. Biochem.* **3993**, *212*, 657–664.
(11) A detailed spectroscopic study of cyanide interaction to cytochrome $ba_3$ from *T. thermophilus* suggests two cyanide ligands bind, one to iron $a_3$ and the other to $Cu_B$, and the presence of four histidine N donors for the latter: Surerus, K. K.; Oertling, W. A.; Fan, C.; Burgiel, R. J.; Einarsdóttir, O.; Antholine, W. E.; Dyer, R. B.; Hoffman, B. M.; Woodruff, W. H.; Fee, J. A. *Proc. Natl. Acad. Sci. U.S.A.* **1992**, *89*, 3195–3199.

copper environment, and few have been structurally characterized. For instance, porphyrin–Fe–($O_2$) species are well-known in myoglobin, hemoglobin, or model compounds,[12] and compelling evidence for 1:1 Cu–$O_2$ adducts, derived from reaction of $Cu^I$ complexes with $O_2$, has recently been obtained.[13] Valentine and co-workers described a porphyrin–$Fe^{III}$–($O_2^{2-}$) complex with side-on $\eta^2$-peroxo binding,[14] and heme Fe(III)–OOH[15] and Fe(III)–OOR[16] species can be generated in solution. Porphyrin ferryl Fe=O moieties are also well studied, since they are of interest in heme peroxidase and cytochrome P-450 enzymes, as well as porphyrin-complex-mediated oxidation reactions.[17] Aquo–Cu(II) and Cu(II)–$\mu$-hydroxo species are plentiful.[18] Well-described examples of mononuclear Cu(II)–($OH^-$) complexes include $Ba_2[Cu(OH)_6]$[19] and, very recently, $[Cu(Me_6tren)(OH)]^+$ ($Me_6$-tren = tris(*N*,*N*-dimethylethyl)amine).[20]

With an extensive background in studies of copper(I)/dioxygen reactivity and related biomimetic chemistry,[21] we have taken an interest in the dioxygen chemistry and reduction to water occurring at this $Fe_{a3}$–$Cu_B$ site, utilizing an inorganic modeling approach.[22] Critical protein conformational changes and proton-pumping processes are coupled to these molecular metal–complex-mediated reactions involving $O_2$ and reduced products,[23] and it is important to clearly resolve the details and subtleties involved. Most previous attempts at modeling the heme $a_3$–$Cu_B$ site have typically been directed at structural models for the oxidized "resting" state[20,24,25] and not the $O_2$-reduction reaction.[26] Our original approach was to combine reduced ferrous porphyrin and cuprous precursors with $O_2$ so as to allow bridged dinuclear complexes to "self-assemble".[27] The complex $[(F_8\text{-TPP})Fe^{III}\text{-O-}Cu^{II}(TMPA)]^+$ (**3**) is an oxo-bridged porphyrin iron(III)/copper(II) species, the product of dioxygen reaction with equimolar quantities of $[(TMPA)Cu(CH_3CN)]^+$ (**1**) (TMPA = tris(2-pyridylmethyl)-amine) and $(F_8\text{-TPP})Fe(pip)_2$ (**2**) ($F_8$-TPP = tetrakis(2,6-difluorophenyl)porphyrinate(2–); pip = piperidine).[27] Using an acid–base synthetic approach, Lee and Holm[20] have also recently prepared and characterized a complex with similar structure, $[(OEP)Fe\text{-O-}Cu(Me_6tren)]^+$ (OEP = octaethylporphyrinate(2–)). This species and our own complex **3** represent important new structural types in inorganic chemistry, i.e., heterodinuclear oxo-bridged compounds with electronically linked redox-active metal ion complexes of relevance to cytochrome *c* oxidase active site chemistry.[22,28,29] The primary subject of this report is the structural description of **3**,[30] along with detailed characterization of its electronic structure as deduced from Mössbauer spectroscopy and multifield saturation magnetization studies.

## Experimental Section

**Synthesis, Materials, and Methods.** Reagents and solvents used were of commercially available reagent quality unless otherwise stated. Dichloromethane ($CH_2Cl_2$) was stirred with concentrated sulfuric acid for several days and washed with water, sodium carbonate (10%) solution, and water. It was then dried over anhydrous $MgSO_4$ and $CaH_2$ before a final reflux and distillation from $CaH_2$. Acetonitrile ($CH_3CN$) was distilled from $CaH_2$. Anhydrous diethyl ether was prepared by passing reagent-grade solvent through a column of activated alumina. Preparation and handling of air-sensitive materials were carried out under an argon atmosphere using standard Schlenk techniques. Solid samples were stored and transferred, and samples for IR and NMR spectra were prepared in a Vacuum Atmospheres drybox filled with argon.

Elemental analyses were performed by Desert Analytics, Tucson, AZ. Infrared spectra were recorded as Nujol mulls on a Mattson Galaxy FTIR spectrometer. UV–vis spectra were recorded on a Shimadzu UV 160U instrument. All wavelengths are reported in nanometers, and the molar extinction coefficients are listed in parentheses. $^1$H-NMR spectra were obtained at 300 MHz on a Bruker AMX-300 instrument. Chemical shifts are reported as $\delta$ values downfield from an internal standard of $Me_4Si$. $^{19}$F-NMR spectra were obtained at 376 MHz on a Varian XL400 instrument.

**TMPA, $[(TMPA)Cu^I(CH_3CN)](ClO_4)$ (1-$ClO_4$), and $[(TMPA)Cu^{II}(CH_3CN)](ClO_4)_2$ (4-$ClO_4$)** were synthesized according to published procedures.[31]

**($F_8$-TPP)FeCl.** Tetrakis(2,6-difluorophenyl)porphyrin ($F_8$-$TPPH_2$) was prepared by standard pyrrole–arylaldehyde condensation in propionic acid, as reported in previous literature.[32] Pyrrole-deuteriated $F_8$-$TPPH_2$ was prepared by exchanging the pyrrole protons prior to condensation with 2,6-difluorobenzaldehyde, as reported previously.[32c] Incorporation of iron into the porphyrin was accomplished by addition of anhydrous $FeCl_2$ (Fluka) (1.00 g), in ~3-fold molar excess, to a refluxing solution of the porphyrin (2.20 g, 2.91 mmol) in DMF (400 mL) under an argon atmosphere,[33] and subsequent stirring for 1 h. Upon cooling, an equal volume of aqueous 2 M NaCl and concentrated HCl (10 mL) were added to the reaction mixture; this was then stored at −15 °C overnight. The resulting crude solid was collected by filtration, washed several times with water (~500 mL), and air dried for 4–5 h. Purification was accomplished by passage through a silica gel column: trace amounts of the demetalated porphyrin eluted as a pink band with dichloromethane

(12) Collman, J. P.; Halbert, T. R.; Suslick, K. S. In *Metal Ion Activation of Dioxygen* T. G. Spiro, Ed.; Wiley: New York, 1980; pp 1–72. (b) Suslick, K. S.; Reinert, T. J. *J. Chem. Educ.* **1985**, *62*, 974.

(13) (a) Karlin, K. D.; Wei, N.; Jung, B.; Kaderli, S.; Zuberbühler, A. D. *J. Am. Chem. Soc.* **1991**, *113*, 5868. (b) Karlin, K. D.; Wei, N.; Jung, B.; Kaderli, S.; Zuberbühler, A. D. *J. Am. Chem. Soc.* **1993**, *115*, 9506–9514.

(14) McCandlish, E.; Miksztal, A. R.; Nappa, M.; Sprenger, A. Q.; Valentine, J. S.; Stong, J. D.; Spiro, T. G. *J. Am. Chem. Soc.* **1980**, *102*, 4268–4271.

(15) Tajima, K.; Shigematsu, M.; Jinno, J.; Ishizu, K.; Ohya-Nishiguchi, H. *J. Chem. Soc., Chem. Commun.* **1990**, 144–145.

(16) Balch, A. L. *Inorg. Chim. Acta* **1992**, *198–200*, 297–307, and references therein.

(17) (a) Dawson, J. H. *Science* **1988**, *240*, 433. (b) Poulos, T. L.; Raag, R. *FASEB J.* **1992**, *6*, 674. (c) Watanabe, Y.; Groves, J. T. In *Mechanisms of Catalysis*; Sigman, D. S., Ed.; Academic Press, Inc.: San Diego, 1992; Vol. XX, pp 405–452.

(18) Hathaway, B. J. In *Comprehensive Coordination Chemistry*; Wilkinson, G., Ed.; Pergamon: New York, 1987; Vol. 5, Chapter 53, pp 533–774.

(19) Dubler, E.; Korber, P.; Oswald, H. R. *Acta Crystallogr.* **1973**, *B29*, 1929.

(20) Lee, S. C.; Holm, R. H. *J. Am. Chem. Soc.* **1993**, *115*, 5833–5834.

(21) (a) Tyeklár, Z.; Karlin, K. D. *Acc. Chem. Res.* **1989**, *22*, 241–248. (b) Karlin, K. D.; Tyeklár, Z.; Zuberbühler, A. D. In *Bioinorganic Catalysis*; Reedijk, J., Ed.; Marcel Dekker: New York, 1993; Chapter 9, pp 261–315. (c) Tyeklár, Z.; Karlin, K. D. In *Bioinorganic Chemistry of Copper*; Karlin, K. D., Tyeklár, Z., Eds.; Chapman & Hall: New York, 1993; pp 277–291. (d) Karlin, K. D.; Tyeklár, Z. *Adv. Inorg. Biochem.* **1994**, *9*, 123–172.

(22) Karlin, K. D. *Science* **1993**, *261*, 701–708.

(23) Woodruff, W. H. *J. Bioenerg. Biomembr.* **1993**, *25* (2), 177–188.

(24) Kitajima, N. *Adv. Inorg. Chem.* **1992**, *39*, 1–77, and references cited therein.

(25) Other recent model studies: (a) Serr, B. R.; Headford, C. E. L.; Anderson, O. P.; Elliott, C. M.; Spartalian, K.; Fainzilberg, V. E.; Hatfield, W. E.; Rohrs, B. R.; Eaton, S. R.; Eaton, G. E. *Inorg. Chem.* **1992**, *31*, 5450–5465. (b) Casella, L.; Bullotti, M. In *Bioinorganic Chemistry of Copper*; Karlin, K. D., Tyeklár, Z., Eds.; Chapman & Hall: New York, 1993; pp 292–305. (c) Wang, R.; Brewer, G. *Inorg. Chim. Acta* **1993**, *206*, 117–121.

(26) For one such study, see: Berry, K. J.; Gunter, M. J.; Murray, K. S. In *Oxygen and Life*; Second BOC Priestley Conference, Birmingham, U.K., Sept 1980; Spec. Publ. No. 39; The Royal Society of Chemistry: London, U.K., pp 170–179.

(27) (a) Nanthakumar, A.; Nasir, M. S.; Karlin, K. D.; Ravi, N.; Huynh, B. H. *J. Am. Chem. Soc.* **1992**, *114*, 6564–6566, and references cited therein. (b) In this report, we incorrectly assigned complex **3** as a peroxo-bridged complex.

(28) For a review of homo and heteronuclear oxo-bridged transition metal complexes, see: West, B. O. *Polyhedron* **1989**, *3*, 219–274.

(29) An oxo bridge previously was suggested as a possibility for the oxidized couple "resting"-state enzyme: (a) Blumberg, W. E.; Peisach, J. In *Cytochrome Oxidase*; King, T., *et al.*, Eds.; Elsevier/North-Holland Biomedical Press: Amsterdam, the Netherlands, 1979; pp 153–159. (b) Reed, C. A.; Landrum, J. T. *FEBS Lett.* **1979**, *106*, 265–267.

(30) A preliminary report of the structure of **3** has been published, with details (i.e., positional and isotropic thermal parameters) available as supplementary material: Nanthakumar, A.; Fox, S.; Murthy, N. N.; Karlin, K. D.; Ravi, N.; Huynh, B. H.; Orosz, R. D.; Day, E. P.; Hagen, K. S.; Blackburn, N. J. *J. Am. Chem. Soc.* **1993**, *115*, 8513–8514.

(31) (a) Tyeklár, Z.; Jacobson, R. R.; Wei, N.; Murthy, N. N.; Zubieta, J.; Karlin, K. D. *J. Am. Chem. Soc.* **1993**, *115*, 2677–2689. (b) Jacobson, R. R.; Tyeklár, Z.; Farooq, A.; Karlin, K. D.; Liu, S.; Zubieta, J. *J. Am. Chem. Soc.* **1988**, *110*, 3690–3692. (c) Jacobson, R. R. Ph.D. Dissertation, State University of New York, Albany, 1989.

(32) (a) Fuhrhop, J.-H.; Smith, K. M. In *Porphyrins and Metalloporphyrins*; Smith, K. M., Ed.; Elsevier: New York, 1975; pp 769–770. (b) Adler, A. D.; Longo, F. R.; Finarelli, J. D.; Goldmacher, J.; Assour, J.; Korsakoff, L. *J. Org. Chem.* **1967**, *32*, 476. (c) Nanthakumar, A.; Goff, H. M. *Inorg. Chem.* **1991**, *30*, 4460–4464.

(33) Adler, A. D.; Longo, F. R.; Varadi, V. *Inorg. Synth.* **1976**, *16*, 213–220.

as eluant. The ($F_8$-TPP)FeCl was then eluted as a dark red band using a 5% methanol/dichloromethane solvent mixture; solvent was evaporated from the eluate and the residual microcrystalline solid dried *in vacuo* overnight (1.959 g, 79%). $^1$H-NMR ($CDCl_3$): $\delta$ 81.0 (pyrrole, v br), 13.5, 12.7 (*meta*-phenyl) and 7.6 (*para*-phenyl). UV–vis ($CH_2Cl_2$; $\lambda_{max}$, nm ($\epsilon$, $M^{-1}$ $cm^{-1}$)): 365 sh (52 700), 412 (108 000), 504 (11 800), 576 (4300), 639 (4300). Anal. Calcd for $C_{44}H_{20}F_8FeN_4Cl$: C, 62.26; H, 2.36; N, 6.60. Found: C, 62.39; H, 2.33; N, 6.37.

**($F_8$-TPP)Fe(pip)$_2$ (2).** The method employed was similar to that reported by Epstein *et al.*[34] A red-brown solution of ($F_8$-TPP)FeCl (300 mg, 0.354 mmol) in $CH_2Cl_2$ (35 mL) was warmed in a water bath until the solvent began to boil. Piperidine (excess, 1.2 mL) was added slowly along the side of the flask while the porphyrin solution was being stirred. The solution immediately turned bright red in color; methanol (75 mL) was then added to the warm solution to yield a purple solid, which was promptly collected by filtration and dried *in vacuo* for 48 h to give 0.210 g (60%) of microcrystalline product. $^1$H NMR ($CD_2Cl_2$): $\delta$ 7.55 (pyrrole, 8 H), 7.20 (phenyl, 12 H). Anal. Calcd for $C_{54}H_{42}F_8FeN_6$: C, 65.97; H, 4.31; N, 8.55. Found: C, 65.42; H, 3.99; N, 8.01.

**[($F_8$-TPP)Fe-O-Cu(TMPA)]($ClO_4$) (3-$ClO_4$).** Under a flow of argon, ($F_8$-TPP)Fe(pip)$_2$ (0.344 g, 0.350 mmol) and [(TMPA)Cu($CH_3CN$)]($ClO_4$) (0.170 g, 0.345 mmol) were added to a Schlenk flask (200 mL) containing oxygen-saturated $CH_2Cl_2$ (25 mL) immersed in a cold bath (–80 °C). The purple solution was stirred at –80 °C for 5 min and allowed to warm slowly to room temperature. The completion of the reaction was confirmed by monitoring the UV–vis spectra of the reaction solution mixture. Crude product (0.315 g, 70%) was obtained by precipitation with heptane (75 mL); this was dissolved in $CH_3CN$ (30 mL), filtered into a 200-mL Schlenk flask, layered with diethyl ether (150 mL), and allowed to stand for a period of 16 h. Red-purple microcrystalline material was then deposited on the sides of the flask; this was collected by decantation of the supernatant followed by drying *in vacuo* for 24 h (0.182 g, 40%). $^1$H NMR ($CD_3CN$): $\delta$ 65.0 (v br, pyrrole), 9.6, 9.2 (*meta*-phenyl, 8 H), 7.8 (*para*-phenyl, 4 H), 4.5 (3 H), –6.8 (v br), –21.5 (3 H), –104.0 (v br). UV–vis: ($CH_3CN$; $\lambda_{max}$, nm ($\epsilon$, $M^{-1}$ $cm^{-1}$)): 322 (33 200), 370 sh (41 500), 434 (131 000), 554 (19 000), 628 (2200), 735 (1070). IR (Nujol, $cm^{-1}$): 1090 (vs, $ClO_4$). Anal. Calcd for $C_{62}H_{38}ClCuF_8FeN_8O_5$: C, 58.12; H, 2.96; N, 8.74. Found: C, 58.55; H, 2.76; N, 8.84.

**($F_8$-TPP)FeOH (5).** In $CH_2Cl_2$ (75 mL) was dissolved ($F_8$-TPP)FeCl (0.200 g, 0.236 mmol). This was stirred with an equal volume of aqueous 0.5 M NaOH for a period of 3–4 h. The completion of the reaction was indicated by UV–vis spectroscopy. The organic layer was separated, and heptane (150 mL) was added slowly to precipitate the porphyrin product (0.105 g, 54%). $^1$H NMR ($CDCl_3$): $\delta$ 81.0 (v br, pyrrole H), 11.4, 10.4 (*meta*-phenyl) and 7.3 (*para*-phenyl). UV–vis ($CH_2Cl_2$; $\lambda_{max}$, nm ($\epsilon$, $M^{-1}$ $cm^{-1}$)): 331 (37 700), 408 (110 500), 572 (11 500). Anal. Calcd for $C_{44}H_{21}F_8FeN_4O$: C, 63.65; H, 2.53; N, 6.75. Found: C, 63.74; H, 2.58; N, 7.11.

**[($F_8$-TPP)Fe]$_2$O.** This synthesis was performed using a procedure analogous to that previously described.[32c] First, ($F_8$-TPP)FeCl (0.200 g, 0.236 mmol) in $CH_2Cl_2$ (75 mL) was stirred with an equal volume of 1 M perchloric acid for 1 h to generate ($F_8$-TPP)Fe$ClO_4$. The organic layer was separated and then shaken with distilled water to instantly generate a red solution of [($F_8$-TPP)Fe]$_2$O. Separation was followed by addition of heptane (150 mL) to precipitate red microcrystalline product (0.232 g, 60%). $^1$H NMR ($CDCl_3$): $\delta$ 13.9 (pyrrole), 7.6 (phenyl). UV–vis ($CH_2Cl_2$; $\lambda_{max}$, nm ($\epsilon$, $M^{-1}$ $cm^{-1}$)): 320 (30 600), 400 (82 600), 561 (9900). Molar absorptivity values are reported per iron.

**Mössbauer Spectroscopy.** Mössbauer spectra were recorded either on a weak-field Mössbauer spectrometer equipped with a Janis 8DT variable-temperature cryostat or on a strong-field Mössbauer spectrometer equipped with a Janis 12 CNDT/SC SuperVaritemp cryostat containing an 8-T superconducting magnet. Both spectrometers were operated in a constant acceleration mode in a transmission geometry. The zero velocity of the Mössbauer spectra is referred to the centroid of the room temperature spectrum of a metallic iron foil.

**Magnetic Measurements. General.** Magnetization measurements were made using a Quantum Design MPMS superconducting susceptometer controlled by a Hewlett-Packard Vectra ES computer running version 2.13 of the MPMS data acquisition software. The manufacturer modified the susceptometer to produce a continuous flow of helium gas through the sample space during measurements. This modification minimizes scatter in magnetization data collected on frozen samples in open holders.

(34) Epstein, L. M.; Straub, D. K.; Maricondi, C. *Inorg. Chem.* **1967**, *6*, 1720–1724.

Data analysis was performed using version 2.54 of the computer program WMAG (available from WEB Research Co., Edina, MN) running on i486DX-based personal computers. Monte Carlo simulations were carried out using the X Window version 2.54 of WMAG on a Hewlett-Packard 9000/730 workstation. The data analysis methods have been described recently.[35]

**Solution Measurements.** Solutions were prepared inside a Vacuum Atmospheres glovebox under argon with the continuously monitored $O_2$ level less than 1 ppm. A freshly opened bottle of reagent-grade acetonitrile was degassed with argon and used without further purification. Because of the large magnetization signal from the dinuclear complex, hysteresis from the slowly relaxing solvent protons did not interfere with the measurements. A 1 mM solution (200 $\mu$L) and 200 $\mu$L of a blank solvent control were each loaded into quartz sample holders and immediately frozen in liquid nitrogen. The quartz holders had been etched overnight in 10% hydrofluoric acid to remove ferromagnetic impurities. The MPMS sample space was set to a temperature of 200 K and the sample loaded directly from a hand dewar of liquid nitrogen into the instrument. This was followed by three evacuate/refill cycles, each of which consisted of four automatic pump/refill cycles. Magnetization data were collected from 2 to 200 K, at applied fields of 0.2, 1.0, 1.5, 2.4, 3.6, and 5.5 T. (This is the amount of data that can be collected over this temperature range in just under 24 h). The data were examined before removing the sample from the instrument and repeated at a particular field if necessary. In order to check for hysteresis in the data, half of the data points in the 2–33 K temperature range were collected while cooling to 2 K. The remaining half of the data points in that temperature range were collected by warming from 2 K. When hysteresis is present, this procedure results in offsets between neighboring points in plots of magnetization against temperature or inverse temperature. No hysteresis was found that was large enough to affect the interpretation of the data.

**Solid Measurements.** A two-piece sample holder was machined from Delrin and soaked for several days in concentrated aqueous HF solution to remove ferromagnetic impurities. Data for the control were collected on the empty holder centered in a plastic straw. The straw was long enough so that neither end was detected by the pickup coil during a measurement scan of the holder. The magnetization data were collected from 2 to 300 K, at applied fields of 0.2, 1.0, 1.8, 3.1, and 5.5 T. (This is the amount of data that can be collected over this large temperature range in just under 24 h.) The holder was then filled with 32.4 mg (25.0 $\mu$mol) of solid sample compressed tightly with a Teflon syringe plunger. Data on the sample were collected as described above for the control.

**X-ray Structure Determination of [($F_8$-TPP)Fe-O-Cu(TMPA)]($ClO_4$)·3$C_7H_8$·2$CH_3CN$ ((3-$ClO_4$)·3$C_7H_8$·2$CH_3CN$) and [($F_8$-TPP)Fe]$_2$O·3$C_7H_8$.** Recrystallization of 3-$ClO_4$ from acetonitrile/toluene at –20 °C under argon gave large purplish-orange crystals suitable for X-ray diffraction, while crystals of [($F_8$-TPP)Fe]$_2$O were obtained from $CH_2Cl_2$/toluene. The automatic centering and least-squares routines were carried out on 25 reflections in the $2\theta$ range 10.7–15.7° for (3-$ClO_4$), 10.44–16.07° for [($F_8$-TPP)Fe]$_2$O. The $\omega$-data-collection technique was used, and data were collected ($3.5° \leq 2\theta \leq 50°$) at a scan speed of 8.0° $min^{-1}$.

The structures were solved by direct methods. The non-hydrogen atoms were refined anisotropically by full-matrix least-squares technique. In 3-$ClO_4$, three toluene and two acetonitrile solvate molecules were identified and all the solvates except one, toluene, behaved normally. [($F_8$-TPP)Fe]$_2$O possesses three molecules of toluene solvate, and all the carbon atoms of these solvates exhibit high thermal parameters. The positions of these atoms were fixed in the final stages of refinement. All hydrogen atoms, except those of toluene molecules, were fixed at calculated positions.

All measurements were made on a Rigaku AFC6S diffractometer at –90 °C using Mo K$\alpha$ ($\lambda$ = 0.710 69 Å) radiation with a graphite monochromator. All calculations were performed using the TEXSAN crystallographic software package on a VAX 3520 computer. Details of crystal and refinement data for both structures are given in Table 1. Other pertinent X-ray data are given in ref 30 or in the supplementary material.

## Results and Discussion

**Synthesis.** The combination of equimolar amounts of [(TMPA)Cu$^I$($CH_3CN$)]$^+$ (**1**) and ($F_8$-TPP)Fe$^{II}$(pip)$_2$ (**2**) in $CH_2Cl_2$, when saturated with dry $O_2$ at –80 °C, gave a purple-red solution upon slow warming to 0 °C. The addition of heptane

(35) Day, E. P. *Methods Enzymol.* **1993**, *227*, 437–463.

**Table 1.** Selected Crystal and Refinement Data for (3-ClO4)·3C7H8·2CH3CN and [(F8-TPP)Fe]2O·3C7H8

| | (3-ClO4)·3C7H8·2CH3CN | [(F8-TPP)Fe]2O·3C7H8 |
|---|---|---|
| formula | $C_{87}H_{68}N_{10}O_5ClF_8FeCu$ | $C_{121}H_{63}N_8OF_{16}Fe_2$ |
| temp, K | 183 | 183 |
| MW | 1640.39 | 2060.53 |
| cryst system | orthorhombic | monoclinic |
| space group | $P2_12_12_1$ | $C2/c$ |
| $a$, Å | 20.017(7) | 21.935(5) |
| $b$, Å | 24.530(8) | 18.010(6) |
| $c$, Å | 15.451(4) | 25.418(9) |
| $\alpha$, deg | 90.00 | 90.00 |
| $\beta$, deg | 90.00 | 95.96(2) |
| $\gamma$, deg | 90.00 | 90.00 |
| $V$, Å$^3$ | 7587(4) | 9987(5) |
| $F$(000) | 3376 | 4184 |
| $Z$ | 4 | 4 |
| $D_{calcd}$, g/cm$^3$ | 1.44 | 1.44 |
| abs coeff, cm$^{-1}$ | 5.85 | 3.73 |
| reflcns collected | 7344 | 9337 |
| independent reflcns | 4915 ($\geq 3\sigma(I)$) | 3620 ($\geq 3\sigma(I)$) |
| no. of refined params | 928 | 573 |
| largest peak/hole,e Å$^{-3}$ | 0.52/−0.63 | 0.70/−0.47 |
| $R^a$ | 0.050 | 0.069 |
| $R_w^b$ | 0.054 | 0.090 |

$^a$ $R = \sum[|F_o| - |F_c|/\sum|F_o|]$. $^b$ $R_w = [\sum w(|F_o| - |F_c|)^2/\sum w|F_o|^2]^{1/2}$, $w = 4F_o^2/\sigma^2(F_o^2)$.

**Scheme 2**

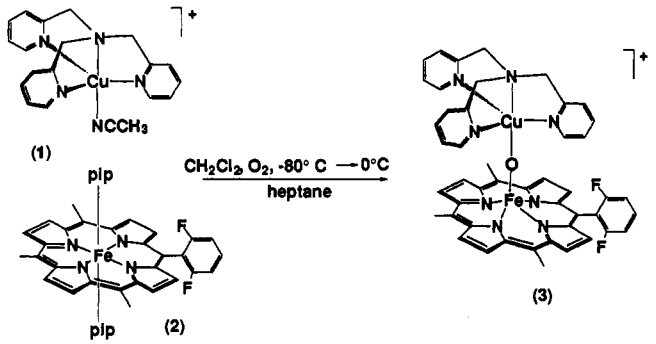


caused precipitation of the oxo-bridged title complex [(F8-TPP)-Fe-O-Cu(TMPA)]+ (**3**) as a reddish-purple solid, in 70% yield (Scheme 2). This complex was also obtained *via* the acid–base reaction of [(TMPA)Cu(CH3CN)]2+ (**4**) and (F8-TPP)Fe$^{III}$-OH (**5**) with triethylamine in CH3CN;[30] further details concerning this latter chemistry will be described elsewhere. Complex **3**-ClO4 dissolves in CH2Cl2, CH3CN, and DMSO and is sparingly soluble in toluene and benzene. Immediate decomposition occurs in protic solvents such as methanol. Crystals of **3**-ClO4 suitable for X-ray structure determination were grown from CH3CN/toluene at −20 °C; microcrystalline material of analytical purity suitable for Mössbauer and EXAFS spectroscopy and multifield saturation magnetization measurements was obtained by slow precipitation from CH3CN/Et2O.

**X-ray Structure.** The title complex, as the perchlorate salt and solvate, [(F8-TPP)Fe-O-Cu(TMPA)](ClO4)·2CH3CN·3C7H8 (**3**-ClO4·2CH3CN·3C7H8), was crystallized from CH3CN/toluene at −20 °C. The structure[30] of the cationic portion **3** (Figure 2) shows the square-pyramidal ferric–porphyrin bridged through its apical ligand (the oxo group) to the distorted square-pyramidal cupric species, which has one of its pyridyl groups serving as the apical donor. As evidenced in the top view of Figure 2, looking down the N1–Cu1–O1–Fe1 near-linear vector shows how the three pyridyl groups of TMPA sit directly above three of the four pyrroles in the F8-TPP ligand, "slotted" between corresponding phenyl groups, thereby leaving one vacant slot. Moreover, the square-pyramidal geometry about Cu1 is quite apparent in Figure 2, with N3 constituting the apex and N1, N2, O1, and N4 the base of the pyramid. From the crystal coordinates,[30] one observes that Cu1 lies 0.11 Å above this basal (least-squares) plane. This places the one d vacancy for the d$^9$ cupric ion in the $d_{x^2-y^2}$ orbital, which is directed toward the ligating atoms N1, N2, and N4 and notably the bridging oxo-atom O1. Thus, the Cu(II) unpaired electron can electronically couple to the porphyrin–iron(III) moiety, by virtue of the bridging of this $O^{2-}$ ligand, *vide infra*.

In Table 2, relevant bond distances and angles observed in [(F8-TPP)Fe-O-Cu(TMPA)]+ (**3**) are compared to other [Cu$^{II}$-(L)X]$^{n+}$ complexes, where L is the tetradentate tripodal ligand TMPA or Me6tren and X is the fifth ligand in the Cu(II) coordination sphere. A comparison of **3** with other $\mu$-oxo ferric–porphyrins is given in Table 3. It is apparent from Table 2 that when L = TMPA and X = Cl$^-$, CH3CN, and $\mu$-1,2-$O_2^{2-}$, essentially trigonal-bipyramidal (TBP) coordination occurs, as measured by the empirical structural parameter $\tau$, which is 1.0 for TBP, but equals 0.0 for a square-based pyramidal (SP) geometry.[36] The axial ligands are X and the tertiary amine "capping" nitrogen of TMPA. In these complexes, the three equatorial Cu–N(py) distances range from 2.035(6) to 2.102(6) Å. For the bridging carbonato complex [{(TMPA)Cu}2(CO3)]2+, however, $\tau$ = 0.47, which indicates a structure intermediate between SP and TBP geometries. For **3**, one of the Cu–N(py) bonds (2.172(7) Å) is markedly longer than the other two, and this constitutes the apical bond of a distorted square-pyramid ($\tau$ = 0.30). The base of the pyramid then comprises the two shorter Cu–N(py) bonds (2.009(7), 1.984(8) Å), the Cu–N(amine) bond (2.100(7) Å), and the Cu–O (of $\mu$-O$^{2-}$) bond (1.856(5) Å). Coincidentally, this short Cu$^{II}$–O distance is virtually identical to that found in the $\mu$-peroxo complex [{(TMPA)Cu}2(O2)]2+,[31] where Cu–O = 1.852(5) Å, although the hybridization about oxygen is sp in **3** (Cu–O–Fe = 178.2(4)°) but sp$^3$ in [{(TMPA)-Cu}2(O2)]2+ (Cu–O–O′ = 107.7(2)°); these differences are too great to justify any meaningful correlation or comparisons between these two species. For [{(TMPA)Cu}2(CO3)]2+,[37] however, where O is approximately sp$^3$ hybridized (Cu–O–C = 113.7(8)°), the Cu–O distance is 1.920(7) Å; this increase versus [{(TMPA)-Cu}2(O2)]2+ may be a consequence of the distorted square-pyramidal coordination in [{(TMPA)Cu}2(CO3)]2+, which is distinct from the virtual trigonal-bipyramidal geometry of [{(TMPA)Cu}2(O2)]2+. The short Cu–O distance in **3** does compare closely to the value of 1.875(4) Å found in the mononuclear Cu(II) hydroxide complex [Cu(Me6tren)(OH)]+ [20] (Table 2). While a number of complexes suggested to contain the $\mu$-oxo Cu(II)–O–Cu(II) core have been reported,[28,38,39] none have been structurally characterized, precluding comparisons with **3**.

Since we were utilizing the fluorinated tetraphenylporphyrin F8-TPP for the generation of complex [(F8-TPP)Fe-O-Cu-(TMPA)]+ (**3**) and others,[30] we also synthesized the $\mu$-oxo dimer [(F8-TPP)Fe]2O, for comparison of oxo–iron and porphyrin–iron structural parameters. Figure 3 displays the crystallographically determined structure, details of which are given in the supplementary material; relevant bonding parameters are found in Table 3. Examination of Table 3 reveals very little difference between $\mu$-oxo dimers [(TPP)Fe]2O[41] and [(F8-TPP)-Fe]2O. The Fe–O–Fe angles are 174.5(1) and 178.5(8)°, respectively, while the Fe–O distances (1.763(1), 1.760(2) Å),

(36) Addison, A. W.; Rao, T. N.; Reedijk, J.; van Rijn, J.; Verschoor, G. C. *J. Chem. Soc., Dalton Trans.* **1984**, 1349–1356.
(37) Tyeklár, Z.; Paul, P. P.; Jacobson, R. R.; Farooq, A.; Karlin, K. D.; Zubieta, J. *J. Am. Chem. Soc.* **1989**, *111*, 388–389.
(38) Sanyal, I.; Mahroof-Tahir, M.; Nasir, M. S.; Ghosh, P.; Cohen, B. I.; Gultneh, Y.; Cruse, R. W.; Farooq, A.; Liu, S.; Zubieta, J. *Inorg. Chem.* **1992**, *31*, 4322–4332, and references cited therein.
(39) Paul, P. P.; Karlin, K. D. *J. Am. Chem. Soc.* **1991**, *113*, 6331–6332.
(40) Karlin, K. D.; Hayes, J. C.; Juen, S.; Hutchinson, J. P.; Zubieta, J. *Inorg. Chem.* **1982**, *21*, 4106–4108.
(41) Hoffman, A. B.; Collins, D. M.; Day, V. W.; Fleischer, E. B.; Srivastava, T. S.; Hoard, J. L. *J. Am. Chem. Soc.* **1972**, *94*, 3620.

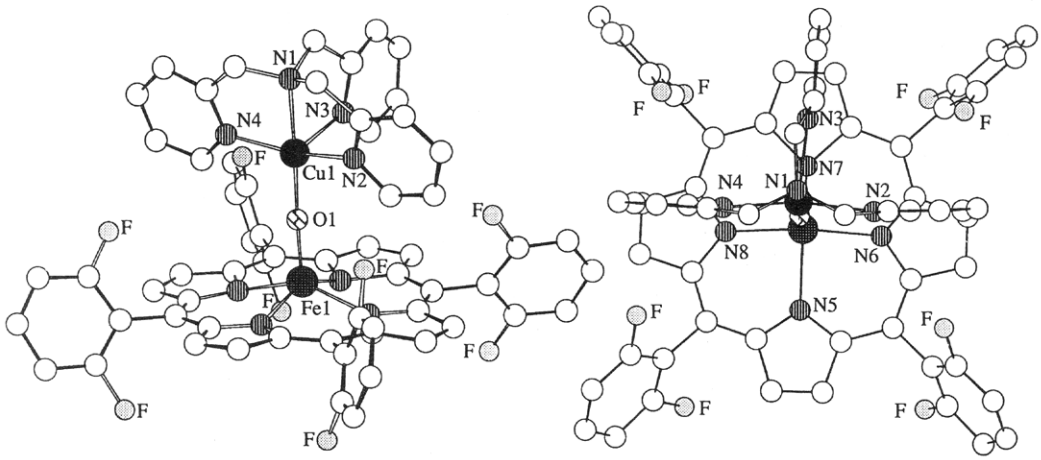


**Figure 2.** Chem 3-D drawings (side and top views) of the oxo-bridged heteronuclear cation $[(F_8\text{-TPP})Fe^{III}\text{-O-}Cu^{II}(TMPA)]^+$ (**3**).

**Table 2.** Comparison of Five-Coordinate Complexes $[Cu^{II}(L)X]^{n+}$: Bond Distances (Å) and Angles (deg)

| | L, X | | | | | | |
|---|---|---|---|---|---|---|---|
| | TMPA, $Cl^-$ | TMPA, $CH_3CN$ | TMPA, $O(\mu\text{-}CO_3^{2-})$ | TMPA, $O(\mu\text{-}1,2\text{-}O_2^{2-})$ | TMPA, $O(\mu\text{-}O^{2-})$ (**3**) | $Me_6$tren, $O(\mu\text{-}O^{2-})^a$ | $Me_6$tren, $OH^-$ |
| Cu–N(capping) | 2.050(6) | 2.019(6) | 2.075(9) | 2.104(6) | 2.100(7) | 2.050(8) | |
| Cu–X | 2.233(2) | 1.978(7) | 1.920(7) | 1.852(5) | 1.856(5) | 1.827(6) | 1.875(4) |
| Cu–N(tripod arm) | 2.062(8) | 2.055(7) | 2.002(8) | 2.102(6) | 2.009(7) | | |
| | 2.060(9) | 2.079(6) | 2.218(10) | 2.024(7) | 2.172(7) | 2.14(2) | |
| | 2.072(6) | 2.035(6) | 1.996(9) | 2.082(7) | 1.984(8) | | |
| N(capping)–Cu–X | 179.1(4) | 178.1(2) | 178.8(3) | 173.7(3) | 176.7(3) | | |
| $\tau$ | 1.00 | 0.96 | 0.47 | 0.86 | 0.30 | 0.91 | |
| reference | 31c, 40 | 31c | 37 | 31 | this work | 20 | 20 |

[a] In complex $[(OEP)Fe\text{-O-}Cu(Me_6tren)]^+$, ref 20.

**Table 3.** Comparison of $\mu$-Oxo-Ferric-Porphyrins: Distances (Å) and Angles (deg)

| | $[(TPP)Fe]_2O$ | $[(F_8\text{-TPP})Fe]_2O$ | $[(F_8\text{-TPP})Fe\text{-O-}Cu(TMPA)]^+$ (**3**) | $[(OEP)Fe\text{-O-}Cu(Me_6tren)]^+$ |
|---|---|---|---|---|
| Fe–O | 1.763(1) | 1.760(2) | 1.740(5) | 1.747(6) |
| Fe–O–M | 174.5(1) | 178.5(8) | 178.2(4) | 176.0(7) |
| Fe–N | 2.087(4) | 2.079(9) | 2.117(6) | |
| | 2.094(6) | 2.085(9) | 2.104(7) | |
| | 2.090(5) | 2.084(9) | 2.102(7) | |
| | 2.076(5) | 2.080(10) | 2.099(7) | |
| Fe–N(average) | 2.087(5) | 2.082(9) | 2.106(7) | 2.109(7) |
| Fe···M | 3.516 | 3.518(3) | 3.596(2) | 3.571(2) |
| Fe–$N_4$ plane (mean) | 0.50 | 0.51 | 0.55 | |
| Fe–porphyrin mean plane | | 0.60 | 0.57 | 0.67 |
| reference | 41 | this work | this work | 20 |

average Fe–N distances (2.087(5), 2.082(9) Å), and $Fe\text{–}N_{plane}$ deviations (0.50, 0.51 Å) (where $Fe\text{–}N_{plane}$ signifies the distance of the iron atom from the mean plane of the four pyrrole nitrogens) are essentially identical and consistent with high-spin Fe(III) porphyrins.[42]

For $[(F_8\text{-TPP})Fe\text{-O-}Cu(TMPA)]^+$ (**3**) there are perhaps slight, but seemingly significant, differences: namely, the slightly shorter Fe–O distance of 1.740(5) Å, the longer Fe–N (average) distance of 2.106(7) Å, and consequently, the longer $Fe\text{–}N_{plane}$ deviation of 0.55 Å. These structural features are consistent with high-spin Fe(III) in **3**. The differences observed in **3** and $[(F_8\text{-TPP})Fe]_2O$ may reflect the diminished $\pi$-accepting ability of Cu(II) ($d^9$) versus high-spin Fe(III) ($d^5$), which has the singly occupied $d_{xz}$ and $d_{yz}$ orbitals of $\pi$ symmetry; this allows the $\mu$-oxo ligand, considered as $O^{2-}$ (having two filled orbitals for $\pi$ bonding), to donate more $\pi$ charge onto the available Fe(III) ion and thereby shorten the Fe–O bond. As mentioned earlier in this discussion, the Cu(II) in complex **3** has its d vacancy in the $d_{x^2-y^2}$ orbital (i.e., along the direction of the ligands), which cannot participate in $\pi$ bonding with the oxo donor. Thus, considerable p orbital electron density remains on the $\mu$-oxo ligand in the Fe-O-Cu complex **3**, at least relative to $\mu$-oxo dimers $[(TPP)Fe]_2O$ and $[(F_8\text{-TPP})Fe]_2O$, which thereby should endow it with enhanced basicity. Relative to most high-spin porphyrin–iron(III) complexes, **3** exhibits a red-shifted Soret band at 434 nm (400 nm for $[(F_8\text{-TPP})Fe]_2O$), consistent with an axial ligand (i.e., the oxo group) with a larger negative charge.[27a] In fact, one might best consider **3** as an adduct of the Lewis base $[(F_8\text{-TPP})Fe^{III}{=}O{:}]^-$, with $[Cu(TMPA)]^{2+}$, a description which has been used for heterodinuclear $\mu$-oxo metal complexes.[28] We recently demonstrated that $[(F_8\text{-TPP})Fe\text{-O-}Cu(TMPA)]^+$ (**3**) can be readily protonated, affording a $\mu$-hydroxo complex $[(F_8\text{-TPP})Fe\text{-(OH)-}Cu(TMPA)]^{2+}$,[30] indicating that the oxo ligand in **3** is still basic, even when bound to Cu(II).

**$[(F_8\text{-TPP})Fe\text{-O-}Cu(TMPA)]^+$ (3) + $H^+$ → $[(F_8\text{-TPP})Fe\text{-(OH)-}Cu(TMPA)]^{2+}$.** Of course, a most relevant structural comparison for $[(F_8\text{-TPP})Fe\text{-O-}Cu(TMPA)]^+$ (**3**) is with the Lee and Holm complex, $[(OEP)Fe\text{-O-}Cu(Me_6tren)]^+$.[20] The data (Tables 2 and 3) reveal extremely similar structures, involving the essentially linear Fe(III)–oxo–Cu(II) linkage, with short and very comparable Fe–O and Cu–O bond lengths; the Fe···Cu distances are also similar.

(42) An Fe-porphyrin mean plane distance of *ca.* 0.50 Å is consistent with a high-spin Fe(III) assignment; this implies an $Fe\text{–}N_{plane}$ distance of *ca.* 0.45 Å. See: (a) Scheidt, W. R.; Reed, C. A. *Chem. Rev.* **1981**, *81*, 543–555. (b) Phillippi, M. A.; Baenziger, N.; Goff, H. M. *Inorg. Chem.* **1981**, *20*, 3904.

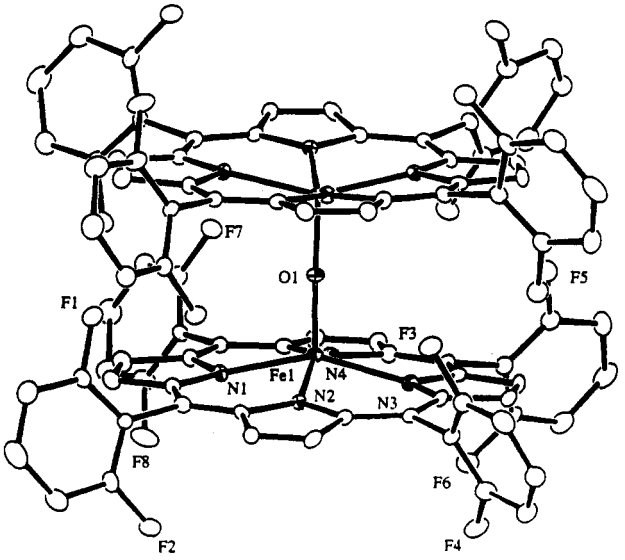


**Figure 3.** ORTEP diagram (15% ellipsoids) of the oxo-bridged diiron(III) complex $[(F_8\text{-TPP})Fe]_2O$. Further structural details are given in the text, Table 3, and the supplementary material.

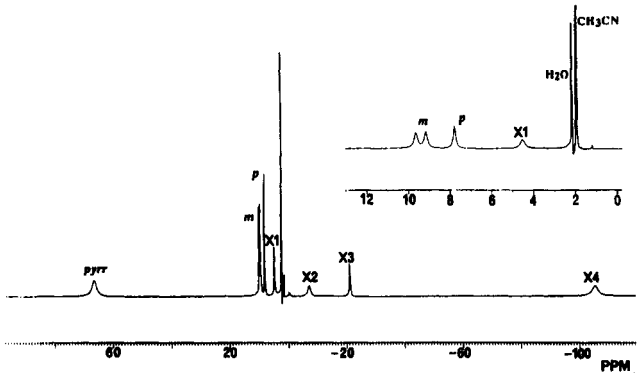


**Figure 4.** $^1$H-NMR spectrum (297 K) of $[(F_8\text{-TPP})Fe\text{-O-Cu(TMPA)}]^+$ (**3**) in $CD_3CN$ solvent. See text for further discussion and assignments.

The geometry about the Cu(II) ion in $[(OEP)Fe\text{-O-Cu}(Me_6\text{-tren})]^+$ is TBP, and the *N*-methyl groups are in van der Waals contact with the porphyrin ring. While this copper ion geometry differs from the more nearly SP geometry in **3** for the Cu–TMPA moiety, the net result in both cases is that the unpaired electron on Cu(II) is in an orbital pointing at the oxo-bridging ligand. Thus, both complexes possess high-spin iron(III) atoms in antiferromagnetically coupled Fe(III)–O–Cu(II) units ($S = 2$ ground state), as discussed for **3** below.

**NMR Spectroscopy.** NMR spectroscopy has proven to be a versatile technique to elucidate the spin and oxidation state of iron in tetraphenylporphyrin complexes.[43] The pyrrole proton NMR signal is expected to be very diagnostic in gauging the extent of magnetic interaction since it exhibits a wide range of chemical shifts in accordance with the iron oxidation and spin state. Previous investigations on a range of Fe/Cu bridged model complexes have usually lacked NMR spectral data to corroborate the proposed extent of magnetic/electronic bridging interactions between the Fe and Cu centers.

The $^1$H-NMR spectrum of $[(F_8\text{-TPP})Fe\text{-O-Cu(TMPA)}]^+$ (**3**) is shown in Figure 4. The $F_8$-TPP meta (*m*) and para (*p*) phenyl hydrogens appear in their usual place. Axially symmetric five-coordinate high-spin (TPP)Fe(III) complexes generally exhibit a pyrrole signal at 80 ppm, whereas the corresponding signal for **3** is shifted in an upfield direction to 65 ppm. This assignment has been confirmed by specific deuteriation of the pyrrole hydrogens in $F_8$-TPP, followed by examination using $^2$H-NMR spectroscopy. Attenuation of the pyrrole chemical shift usually reflects lower contact spin density at the pyrrole carbons. Porphyrin–iron complexes can have a reduced pyrrole shift if there is a reduction in the magnetic moment value as a result of intermediate spin ($S = 3/2$) mixing (e.g., (TPP)Fe-$PF_6$ or (TPP)Fe-$ClO_4$, which have weak axial ligands)[44] and/or antiferromagnetic coupling with another paramagnetic metal center through a bridging ligand (e.g., (TPP)Fe-O-Fe(TPP), $\delta_{pyrrole} \sim 13.5$ ppm; (TPP)Fe-($O_2^{2-}$)-Fe(TPP), $\delta_{pyrrole} \sim 16$ ppm).[45] The possibility of intermediate spin mixing in **3** can be ruled out on the basis of the strongly basic nature of the oxo ligand, as well as spectroscopic data, i.e. the UV–vis data which is not characteristic of an intermediate spin system, structural parameters (*vide supra*), and the Mössbauer and magnetization data, discussed below. High-spin $S = 2$ (TPP)Fe(II) complexes exhibit chemical shifts over a wide range between $\delta = 30$ and 61 ppm.[46] Hence the upfield shift observed for **3** could be rationalized in terms of a coupling mechanism between the high-spin iron(III) ($S = 5/2$) and Cu(II) ($S = 1/2$) to give an $S = 2$ electronic ground state. Variable-temperature measurements show Curie behavior for the pyrrole proton isotropic shift in the region 210–298 K, as expected for either high and/or low values of $-J$, the coupling constant for $\mathcal{H} = -2J\mathbf{S}_1\cdot\mathbf{S}_2$.[47] However, the variation of slope between high and low limits of magnetic coupling is extremely small in the temperature range accessible by NMR solution spectroscopy, so as to render impossible an accurate estimate of the $-J$ value for this particular spin system.[47]

Four additional proton signals labeled X1, X2, X3, and X4 (Figure 4) are tentatively assigned to the TMPA ligand on the copper ion in $[(F_8\text{-TPP})Fe\text{-O-Cu(TMPA)}]^+$ (**3**), on the basis of preliminary deuteriation/methylation experiments. Since monomeric Cu(II) complexes generally do not exhibit well-resolved (observable) proton NMR signals, the presence of these resonances indicates an electronic interaction between the metal centers either through the bridging bonds or through space, so as to induce rapid electronic relaxation.

An $^{19}$F-NMR spectrum of **3** at 298 K shows a split signal ($\delta = 54.3$ and 51.7 ppm upfield from $CFCl_3$), as one would expect for a five-coordinated axially symmetric high-spin iron(III) complex, indicating different magnetic environments (on the NMR time scale at this temperature) for the *ortho*-fluorine atoms on the phenyl groups of $F_8$-TPP in **3**. The corresponding split in the *m*-phenyl protons (Figure 4) is also consistent with this observation.

In summary, the NMR data suggest the structure of **3** is maintained in solution, i.e., with an undissociated coupled Fe(III)–O–Cu(II) complex.

**Mössbauer Spectroscopy: Results.** Mössbauer spectra of solid $[(F_8\text{-TPP})Fe\text{-O-Cu(TMPA)}]^+$ (**3**) are shown in Figure 5. The data were recorded at 4.2 K in the absence of a magnetic field (spectrum A) and in a field of 0.5 T (spectrum B) and 8 T (spectrum C). The fields were applied parallel to the $\gamma$-beam. In the absence of a magnetic field, a very sharp quadrupole doublet is observed, indicating a well-defined iron environment for **3**. A least-squares fit of the zero-field spectrum yields a full width at half-maximum of 0.26 mm/s for both absorption lines and parameters $\Delta E_Q = 1.26 \pm 0.02$ mm/s and $\delta = 0.46 \pm 0.01$ mm/s typical for high-spin ferric heme ($S = 5/2$).[48] The $\Delta E_Q$ is found to be relatively temperature independent, having a value of 1.23 mm/s at 190 K. At 4.2 K, mononuclear high-spin ferric hemes generally exhibit a Mössbauer spectrum with magnetic hyperfine

(43) Goff, H. M. In *Iron Porphyrins*, Part 1; Lever, A. B. P., Gray, H. B., Eds.; Addison-Wesley: Reading, MA, 1983; Chapter 4.

(44) Goff, H. M.; Shimomura, E. *J. Am. Chem. Soc.* **1980**, *102*, 31–37.
(45) Chin, D.-H.; La Mar, G. N.; Balch, A. L. *J. Am. Chem. Soc.* **1980**, *102*, 4344–4349.
(46) Shirazi, A.; Goff, H. M. *J. Am. Chem. Soc.* **1982**, *104*, 6318–6322.
(47) Wojciechowski, W. *Inorg. Chim. Acta* **1967**, *1*, 324–328.
(48) Debrunner, P. *Iron Porphyrins*, Part 3; Lever, A. B. P., Gray, H. B., Eds.; VCH: New York, 1990; pp 139–234.

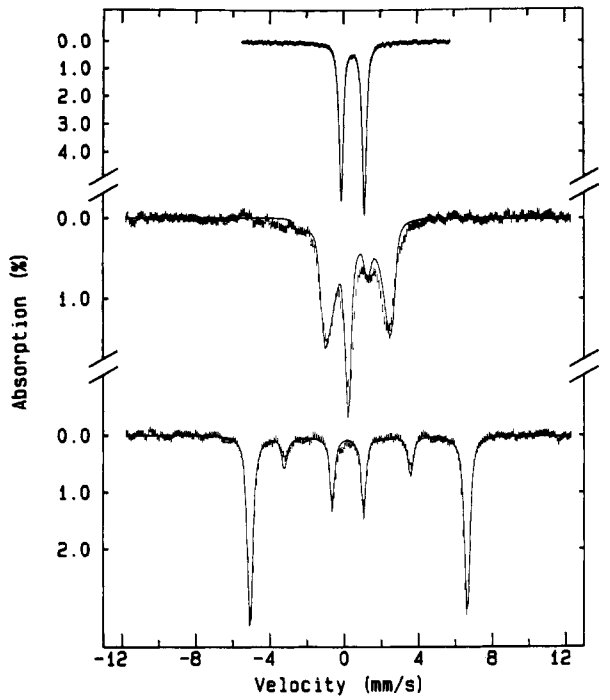


**Figure 5.** Mössbauer spectra of crystalline powder of [($F_8$-TPP)Fe-O-Cu(TMPA)]($ClO_4$) (**3**-$ClO_4$) at 4.2 K. The spectra were recorded in the absence of an applied field (A, top) and in the presence of a magnetic field of 0.5 T (B, middle) and 8 T (C, bottom). The fields were applied parallel to the $\gamma$-beam. The *solid line* in A is a least-squares fit to the data, and the *solid lines* in B and C are theoretical simulations using the parameters quoted in the text.

structure. The observation of a simple quadrupole doublet for **3** indicates that either the heme Fe has a fast electronic relaxation rate or it is magnetically coupled to another half-integer spin center (i.e., the Cu(II)), forming an integer spin system. The latter case is confirmed from the magnetic properties observed in spectra recorded with an applied field (e.g., see Figure 5B). Based on the saturation–magnetization study presented below, the coupling between the heme Fe and Cu is found to be strong and antiferromagnetic, resulting in a system spin $S = 2$. The strong-field Mössbauer spectra were therefore analyzed using the following spin Hamiltonian with $S = 2$ (eq 2). All the

$$\mathcal{H} = D\left[S_z^2 - \frac{S(S+1)}{3} + \frac{E}{D}(S_x^2 - S_y^2)\right] + \beta\vec{S}\cdot\tilde{g}\cdot\vec{H} + \vec{S}\cdot\tilde{A}\cdot\vec{I} + \frac{eQV_{zz}}{4}\left[I_z^2 - I(I+1)/3 + \frac{\eta}{3}(I_x^2 - I_y^2)\right] - g_n\beta_n\vec{H}\cdot\vec{I} \quad (2)$$

parameters in eq 2 can be determined with good accuracy through analysis of the Mössbauer spectra: The magnitude of the quadrupole splitting, the isomer shift, and the line width were determined from a least-squares fit of the zero-field spectrum. The sign of $\Delta E_Q$ and the asymmetry parameter $\eta$ can be obtained from the line positions of the 8-T spectrum. Because the total magnetic splitting of a spectrum is determined by the internal field which is directly proportional to the product $A\langle S\rangle$, the magnetic hyperfine coupling constant $A$ can be estimated from the 8-T spectrum where $\langle S\rangle$ is near its saturation value of 2. At fields less than 8 T, the expectation value $\langle S\rangle$ induced by the applied field through mixing of electronic states is approximately proportional to $A/D$.[49] Consequently, with the $A$ value determined from the 8-T spectrum, the zero-field splitting parameter $D$ can be obtained from spectra recorded with applied fields ranging from 0.5 to 4 T. Other parameters, such as $E/D$, can be determined by comparing theoretical simulations with experimental spectra.

After comparing the experimental data with a series of theoretical simulations, the following set of parameters were determined for [($F_8$-TPP)Fe-O-Cu(TMPA)]$^+$ (**3**): $D = 6.0 \pm 0.5$ cm$^{-1}$, $E/D = 0.03 \pm 0.01$, $\Delta E_Q = -1.26 \pm 0.02$ mm/s, $\eta = 0$, $\delta = 0.46 \pm 0.01$ mm/s, and $A/g_n\beta_n = -23.7 \pm 0.3$ T. This set of parameters yields theoretical simulations in good agreement with experimental spectra recorded in an applied field ranging from 0 to 8 T. The *solid lines* plotted in Figure 5, parts B and C, represent such theoretical simulations. The $D$ value (6 cm$^{-1}$) determined for **3** in the solid form is slightly larger than the value 4.8 cm$^{-1}$ for the solution sample determined from the magnetization study presented below. This difference may be caused by the presence of a weak antiferromagnetic interaction between adjacent molecules in the solid, or it may simply reflect slight structural changes between solid and solution forms of the compound, or both effects may contribute to the difference. A slightly smaller $\Delta E_Q$ of 1.17 mm/s was observed for compound **3** in acetonitrile, suggesting a possible minor structural change.

The above-mentioned parameters are for the electronic state of the coupled Fe(III)–X–Cu(II) system. Assuming antiferromagnetic coupling between the Fe(III) ($S = 5/2$) and Cu(II) ($S = 1/2$) ions, the intrinsic zero-field splitting parameter $D_{Fe}$ and the magnetic hyperfine coupling constant $A_{Fe}$ for the ferric ion can be estimated using the following relationships (eq 3):[50]

$$D_{Fe} = (3/4)D = 4.5 \text{ cm}^{-1} \quad (3)$$

and

$$A_{Fe} = (6/7)A = (-20.3 \text{ T})g_n\beta_n$$

These values are typical for high-spin ferric compounds and are within the range observed for high-spin ferric heme proteins ($D_{Fe}$ = 3.8 to 15 cm$^{-1}$ and $A_{Fe}/g_n\beta_n$ = −22 to −18 T).[48] Most characteristically, the isotropic $A_{Fe}$ value obtained for [($F_8$-TPP)-Fe-O-Cu(TMPA)]$^+$ (**3**) is identical to the value, −20 T, observed for metmyoglobin.[51] On the other hand, the zero-field splitting parameter of **3** falls on the low side of the boundary. Most of the heme proteins have $D_{Fe}$ values above 6 cm$^{-1}$.

**Mössbauer Spectroscopy Discussion.** We have applied Mössbauer spectroscopy to characterize the electronic state of **3**. The data unambiguously indicate that the iron is high-spin ferric ($S_{Fe} = 5/2$). The observed hyperfine parameters, $\Delta E_Q$, $\delta$, $D$, $E/D$, and the isotropic $A$ value, are all characteristic of a high-spin ferric ion. The magnetic properties of the spectra in the absence and presence of a magnetic field demonstrate further that the ferric ion is spin-coupled to the cupric ion forming an integer spin system. Saturation magnetization measurements (*vide infra*) indicate that the ions are strongly antiferromagnetically coupled and the net system spin is $S = 2$. The Mössbauer data are consistent with and corroborate such a spin-coupled scheme. The possibility of an intermediate spin ferric ion ($S_{Fe} = 3/2$) ferromagnetically coupled to a Cu(II) ion forming an $S = 2$ system is precluded by the Mössbauer data, since intermediate spin Fe(III) porphyrin model compounds generally display very large $\Delta E_Q$ (>3 mm/s) and anisotropic $A$.[48,52,53]

Mössbauer spectroscopy has also been applied to study the coupled heme $a_3$–$Cu_B$ site in cytochrome oxidases, and spectral properties similar to that of [($F_8$-TPP)Fe-O-Cu(TMPA)]$^+$ (**3**) were observed.[54-56] Most interestingly, the Mössbauer parameters of **3** compare very well with those observed for the ferric heme

(49) Huynh, B. H.; Münck, E.; Orme-Johnson, W. H. *Biochim. Biophys. Acta* **1979**, *576*, 192–203.

(50) Scaringe, R. P.; Hodgson, D. J.; Hatfield, W. E. *Mol. Phys.* **1978**, *35*, 701–713.

(51) Lang, G. *Q. Rev. Biophys.* **1970**, *3*, 1–60.

(52) Gupta, G. P.; Lang, G.; Scheidt, W. R.; Geiger, D. K.; Reed, C. A. *J. Chem. Phys.* **1986**, *85*, 5212–5220.

(53) Gupta, G. P.; Lang, G.; Reed, C. A.; Shelly, K.; Scheidt, W. R. *J. Chem. Phys.* **1987**, *86*, 5288–5293.

$a_3$ of beef heart cytochrome *c* oxidase ($\Delta E_Q$ = 1.0 mm/s and $\delta$ = 0.48 mm/s)[54] and of cytochrome $c_1aa_3$ from *Thermus thermophilus* ($\Delta E_Q$ = 1.3 mm/s, $\delta$ = 0.41 mm/s, and $A_{Fe}/g_n\beta_n$ = −19 T).[55] For beef heart cytochrome *c* oxidase, $^{57}$Fe enrichment was impossible and only the values of $\Delta E_Q$ and $\delta$ were reported. For the study of the bacterial enzyme, detailed analyses of the data have been performed. Multiple ferric forms of heme $a_3$ were found in the as-isolated cytochrome $c_1aa_3$. The coupling between heme $a_3$ and $Cu_B$ was found to be antiferromagnetic, and the Mössbauer spectra were satisfactorily simulated using either a weak or a strong coupling scheme. In the weak coupling scheme ($|J| \sim 1$ cm$^{-1}$), the $D_{Fe}$ was determined to be +8 cm$^{-1}$, a value that is more commonly observed for high-spin ferric hemes. It was noted, however, by Rusnak *et al.*[55] that a coupling constant of 1 cm$^{-1}$ may not require a bridging ligand. In the strong coupling situation ($|J| > 10$ cm$^{-1}$), a value of ~3 cm$^{-1}$ was found for $D_{Fe}$. This value was judged to be unusually small for high-spin ferric heme.[55] Unfortunately, saturation magnetization measurements were not available to determine the strength of the exchange coupling. In the current study, the observed $D_{Fe}$ value for **3** is small and comparable to that determined for the strong coupling situation in cytochrome $c_1aa_3$, indicating that it may not be unusual for a strongly coupled heme–Cu system to have a small value of $D_{Fe}$.

While the above-mentioned similarities between the model compound and the enzymes are intriguing, the significance is unclear. It is important, however, to point out that even though the magnitude of the $\Delta E_Q$ is similar between [(F₈-TPP)Fe-O-Cu(TMPA)]⁺ (**3**) and cytochrome $c_1aa_3$, the sign of $\Delta E_Q$ for the enzyme is positive while that of **3** is negative, indicating different charge distributions surrounding the two heme irons. The Mössbauer spectroscopic parameters for **3** do closely agree with those for the structurally similar [(OEP)Fe-O-Cu(Me₆tren)]⁺ complex, also with its near-linear $\mu$-oxo bridge, where $\Delta E_Q$ = 1.20 mm/s and $\delta$ = 0.48 mm/s;[20] a more detailed Mössbauer spectroscopic analysis of this compound has not yet been presented. For a number of other model compounds previously speculated to possess oxo-bridged porphyrin–Fe(III)/Cu(II) model moieties, only high-temperature quadrupole splitting and isomer shift have been reported,[57] and therefore, in certain cases, unambiguous assignment of the iron electronic state is difficult. For example, an intermediate spin ($S$ = 3/2) Fe(III) was assigned for a putative $\mu$-oxo-bridged Fe(III) porphyrin–Cu(II) complex,[57c] while the reported Mössbauer parameters ($\Delta E_Q$ = 2.06 mm/s and $\delta$ = 0.23 mm/s) are characteristic for low-spin ferric heme ($S$ = 1/2). Other known oxo-bridged Fe–porphyrin complexes are generally homodimers, which yield a much smaller $\Delta E_Q$ of 0.5–0.7 mm/s.[58]

**Magnetism: Solution Measurements.** The 1 mM solution data for [(F₈-TPP)Fe-O-Cu(TMPA)]⁺ (**3**) were first fit to a strong coupling model using the following spin Hamiltonian (eq 4):

$$\mathcal{H} = D[\mathbf{S}_z^2 - S(S+1)/3 + (E/D)(\mathbf{S}_x^2 - \mathbf{S}_y^2)] + \beta \mathbf{g}\cdot\mathbf{S}\cdot\mathbf{H} \quad (4)$$

with $S$ = 2, where $D$ is the zero-field splitting, $E/D$ is the rhombicity, and $\beta\mathbf{g}\cdot\mathbf{S}\cdot\mathbf{H}$ represents the Zeeman interaction of the magnetic moment with the applied magnetic field. Initial fitting to this model with $D$, $E/D$, and $g$ as free parameters always produced a very small value of $E/D$. On the basis of this observation, and to limit the number of free parameters, axial symmetry ($E/D$ = 0) was assumed for subsequent fits. An excellent fit, shown in Figure 6, to all six fields of data was achieved using this model with $D$ = 4.8 cm$^{-1}$ and $g$ = 1.95. The standard discrepancy was $\chi^2$ = 1.6. The value of $D$ obtained from this fit is the system $D$ value for the $S$ = 2 dimer. The $D$ value for the ferric site ($D_{Fe}$) can be calculated using eq 3.[50] This yields a $D_{Fe}$ value of 3.6 cm$^{-1}$. The same data were next fit to a dimer model. This model is described by the following spin Hamiltonian (eq 5):

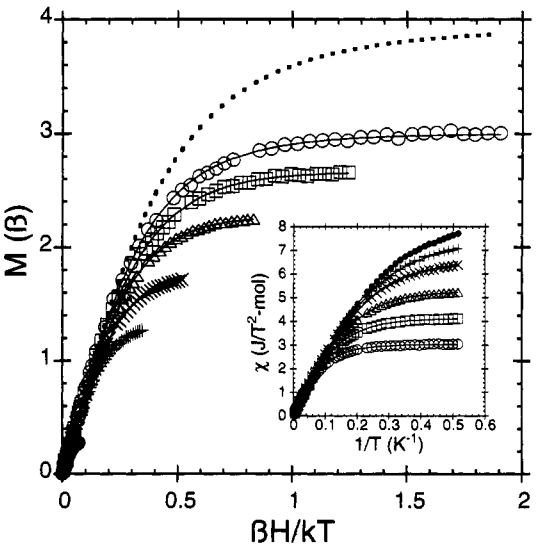


**Figure 6.** Magnetization of a 1 mM solution of [(F₈-TPP)Fe-O-Cu(TMPA)](ClO₄) (**3**-ClO₄) in $CH_3CN$ plotted against $\beta H/kT$, highlighting the low-temperature data. Six fields of data (●, 0.2; +, 1.0; ×, 1.5; △, 2.4; □, 3.6; and ○, 5.5 T) are shown over the temperature range from 2 to 200 K. The solid lines are a theoretical fit to an $S$ = 2 strong coupling model (eq 4) with $E/D$ fixed at 0 and $D$ and $g$ treated as free parameters. The parameter values found from the fit were $D$ = 4.8 cm$^{-1}$ and $g$ = 1.95 with the quality of fit $\chi^2$ = 1.6. The dashed line is the Brillouin curve calculated by assuming $D = E/D = 0$. Because the $g$ value is slightly less than 2, the low-temperature asymptote of the Brillouin curve for this spin $S$ = 2 system is slightly less than 4 $\mu_B$. The inset presents the same data and fit as susceptibility versus inverse temperature in order to exhibit the high quality of the fit to each of the six fields throughout the low-temperature range.

$$\mathcal{H} = -2J\mathbf{S}_1\cdot\mathbf{S}_2 + D_{Fe}[\mathbf{S}_1^2 - S_1(S_1+1)/3 + (E/D)(\mathbf{S}_{1x}^2 - \mathbf{S}_{1y}^2)] + \beta\mathbf{g}_1\cdot\mathbf{S}_1\cdot\mathbf{H} + \beta\mathbf{g}_2\cdot\mathbf{S}_2\cdot\mathbf{H} \quad (5)$$

where $D_{Fe}$ now represents the zero-field splitting at the ferric site, $E/D$ is the rhombicity at the ferric site, and $\mathbf{g}_1$ and $\mathbf{g}_2$ are the $g$ tensors for the ferric and cupric sites, respectively. The first term ($-2J\mathbf{S}_1\cdot\mathbf{S}_2$) represents the exchange coupling between the Fe(III) and Cu(II) sites. The excellent fit that was obtained with the $S$ = 2 monomer model above indicates that the exchange coupling is antiferromagnetic and large. In order to keep the number of free parameters small, the $E/D$ and $g$ values for the ferric site were fixed at 0 and 2.0, respectively, and the $g$ values for the cupric site were fixed at the EPR measured values for [(TMPA)Cu(H₂O)]²⁺,[59] i.e., $g_x$ = 2.198, $g_y$ = 2.198, $g_z$ = 2.004. The quality of the fit was found to be insensitive to the final value of $J$ due to the low signal-to-noise at high temperatures for this 1 mM solution data. Instrument noise does not depend on sample temperature, but the paramagnetic signal decreases with increasing temperature leading to decreasing signal-to-noise at high temperatures. The data are plotted in Figure 7 with theoretical curves corresponding to different values of $J$. It is clear from the

(54) Kent, T. A.; Young, L. J.; Palmer, G.; Fee, J. A.; Münck, E. *J. Biol. Chem.* **1983**, *258*, 8543–8546.
(55) Rusnak, F. M.; Münck, E.; Nitsche, C. I.; Zimmermann, B. H.; Fee, J. A. *J. Biol. Chem.* **1987**, *262*, 16328–16332.
(56) Kent, T. A.; Münck, E.; Dunham, W. R.; Filter, W. F.; Finding, K. L.; Yoshida, T.; Fee, J. A. *J. Biol. Chem.* **1982**, *257*, 12489–12492.
(57) (a) Lukas, B.; Miller, J. R.; Silver, J.; Wilson, M. T.; Morrison, I. E. G. *J. Chem. Soc., Dalton Trans.* **1982**, 1035–1040. (b) Chang, C. K.; Koo, M. S.; Ward, B. *J. Chem. Soc., Chem. Commun.* **1982**, 716–719. (c) Saxton, R. J.; Olson, L. W.; Wilson, L. J. *J. Chem. Soc., Chem. Commun.* **1982**, 984–986.
(58) Kurtz, D. M., Jr. *Chem. Rev.* **1990**, *90*, 585–606.
(59) Jacobson, R. R.; Tyeklár, Z.; Karlin, K. D.; Zubieta, J. *Inorg. Chem.* **1991**, *30*, 2035–2040.

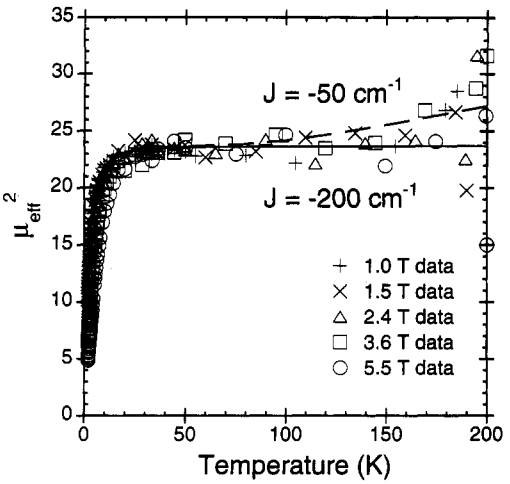


**Figure 7.** Susceptibility of the same solution data as shown in Figure 1 plotted as $\mu_{eff}^2$ versus temperature, highlighting the high-temperature data. The solid lines were calculated assuming an $S = 5/2$, $S = 1/2$ dimer model (eq 5) with $D_{Fe}$ equal to 3.6 $cm^{-1}$, $E/D$ equal to 0, $g$(Fe) equal to 2, $g$(Cu) set to the measured EPR values for $[(TMPA)Cu^{II}(OH_2)]^{2+}$, and $J$ fixed at the indicated values. The quality of fit for either $J$ value was $\chi^2 = 1.85$. Comparison of the theoretical curves with the data illustrates the difficulty due to low signal-to-noise at high temperatures in measuring antiferromagnetic $J$ on a 1 mM spin concentration sample when $|J| > 50$ $cm^{-1}$.

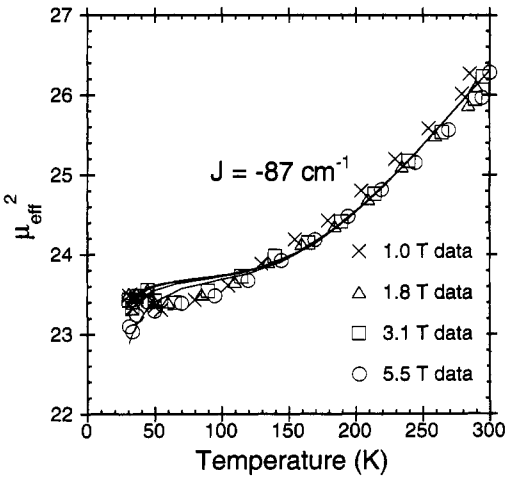


**Figure 8.** Susceptibility of solid $[(F_8\text{-TPP})Fe\text{-O-}Cu(TMPA)](ClO_4)$ (**3**-$ClO_4$), plotted as $\mu_{eff}^2$ versus temperature, showing the high-temperature portion of the data only. The solid lines are a theoretical fit to an $S = 5/2$, $S = 1/2$ dimer model (eq 5) with $D$ fixed at 3.6 $cm^{-1}$, $E/D$ fixed at 0, $g$(Fe) fixed at 2, $g$(Cu) fixed at the measured EPR values for $[Cu^{II}(TMPA)(OH_2)]^{2+}$, and $J$ as a free parameter. The value of $J$ found from the fitting process was $J = -87$ $cm^{-1}$ with $\chi^2 = 2.6$.

figure that low signal-to-noise limits the lower limit on $|J|$ for 1 mM concentrations of a coupled high-spin ferric site with a cupric site to $|J|$ greater than 50 $cm^{-1}$.

**Solid-State Measurements.** In order to improve the quality of the data at high temperatures, measurements were made on the solid. This gave the additional advantage of being able to measure temperatures up to 300 K, instead of the 200 K upper limit for frozen acetonitrile in an open quartz holder. In Figure 8, we show the results of fitting the highest four fields of powder data at temperatures above 30 K with the dimer Hamiltonian (eq 5). Drawing from the fit to the solution data, the ferric $D_{Fe}$, $E/D$, and $g$ values were fixed at 3.6 $cm^{-1}$, 0, and 2.0, respectively. The copper $g$ values were also fixed as before. This gave an excellent fit over the high-temperature range with $J = -87$ $cm^{-1}$ and $\chi^2 = 2.6$.

**Magnetism: Discussion.** We have applied the multifield saturation magnetization technique to both the solid and a 1 mM acetonitrile solution of $[(F_8\text{-TPP})Fe\text{-O-}Cu(TMPA)](ClO_4)$ (**3**-$ClO_4$). Both the solid and solution magnetic data indicate strong antiferromagnetic coupling between the ferric and cupric sites to give an $S = 2$ ground state for the dimer. The exact magnitude of the exchange coupling is difficult to establish from the 1 mM solution data due to low signal-to-noise at high temperatures. Antiferromagnetic coupling between the heme $a_3$ and $Cu_B$ sites in cytochrome *c* oxidase was originally proposed by van Gelder and Beinert to explain the lack of EPR signal from these metal centers.[60] Subsequent magnetic susceptibility studies have confirmed the coupling model in cytochrome *c* oxidase.[61,62] The magnitude of the coupling has been stated as $|J| \geq 200$ $cm^{-1}$; that is, the dinuclear site is fully coupled at room temperature.[61] On the basis of our present studies of 1 mM solutions of the title model compound, which has similar magnetic properties to those of the coupled site of cytochrome *c* oxidase, it is difficult to see how this large a lower limit on the magnitude of the exchange coupling could be determined (a typical maximum working concentration for a protein such as cytochrome *c* oxidase is less than 1 mM). On the basis of our present results (Figure 7) a lower limit of $J$ greater than 50 $cm^{-1}$ would be a better estimate for the exchange coupling in cytochrome *c* oxidase if it is indeed strongly coupled.[55,62]

## Summary/Conclusion

The unusual $\mu$-oxo complex $[(F_8\text{-TPP})Fe^{III}\text{-O-}Cu^{II}(TMPA)]^+$ (**3**) has been isolated in reasonable yield (40%, recrystallized) from the reaction of $[(TMPA)Cu^{I}(CH_3CN)]$ (**1**), $(F_8\text{-TPP})Fe^{II}(pip)_2$ (**2**), and $O_2$ in $CH_2Cl_2$, and as such represents the prototypical, albeit crude, model of cytochrome *c* oxidase *function*, namely, $O_2$-reduction at the reduced Fe(II)/Cu(I) heme $a_3/Cu_B$ to give the oxidized bridged isolated product, Fe(III)–X–Cu(II). We have not as yet elucidated the detailed mechanism of this O–O cleavage reaction, but have shown that the O-bridging atom in **3** is indeed derived from dioxygen.[27a] In isolated mammalian enzyme, the identity of X is not established, but its existence is inferred from the EPR silence and antiferromagnetic coupling observed,[61,62] which necessitates a bridging ligand to mediate electronic interactions between metal ions in this heterodinuclear center. Mössbauer studies of mammalian and bacterial enzyme preparations[54-56] indicate that the dinuclear site consists of high-spin Fe(III) (heme $a_3$) coupled with $Cu(II)_B$ to yield an integer spin ground state. Thus, oxo-bridged complex **3** and $[(OEP)Fe\text{-O-}Cu(Me_6tren)]^+$ [20] are the first model compounds shown to definitively contain such an oxo-bridging ligand and for which distinctive enzyme resting (isolated) state physical properties (i.e., high-spin porphyrin Fe(III), moderate to strong coupling to Cu(II) to give an $S = 2$ heterodinuclear complex) have been duplicated. Thus, if the resting-state enzyme is indeed strongly coupled,[62] then these model compound studies have shown that the oxo bridge is a candidate for the bridging ligand. However, the linear Fe(III)–oxo–Cu(II) moiety in these complexes may not exactly model the structure of this "resting-state" oxidized enzyme, since both EXAFS measurements on mammalian preparations[1e] and recent EXAFS studies carried out on bacterial enzyme implicate a *nonlinear* Fe–X–Cu arrangement,[8] on account of the absence of a strong multiple scattering effect that would have been observed for a linear, or near-linear, Fe–X–Cu moiety.[30] Another notable difference is that the sign of the quadrupole splitting for $[(F_8\text{-TPP})Fe^{III}\text{-O-}Cu^{II}(TMPA)]^+$ (**3**) ($\Delta E_Q = -1.26 \pm 0.02$ mm/s) is opposite that determined for the enzyme (*vide supra*), a clear indication of differing charge distributions. In the near future, it will be interesting and important to compare

(60) van Gelder, B. F.; Beinert, H. *Biochim. Biophys. Acta* **1969**, *189*, 1–24.
(61) Tweedle, M. F.; Wilson, L. J.; Garcia-Iñiguez, L.; Babcock, G. T.; Palmer, G. *J. Biol. Chem.* **1978**, *253*, 8065–8071.
(62) Day, E. P.; Peterson, J.; Sendova, M. S.; Schoonover, J.; Palmer, G. *Biochemistry* **1993**, *32*, 7855–7860.

the physical properties of enzyme states of various bacterial oxidases, now amenable to isolation and manipulation of larger quantitites in purer forms.[2b]

[(F$_8$-TPP)Fe$^{III}$-O-Cu$^{II}$(TMPA)]$^+$ (**3**) displays a linear Fe–O–Cu bridge arrangement with short M–O bonds. The Mössbauer spectroscopic study proves a high-spin Fe(III) assignment and indicates an integer ground state, formed by coupling between high-spin Fe(III) ($S = 5/2$) and Cu(II) ($S = 1/2$). Saturation magnetization studies determine an $S = 2$ ground-state assignment, with strong magnetic coupling, $J = -87$ cm$^{-1}$ for $\mathcal{H} = -2J\mathbf{S_1}\cdot\mathbf{S_2}$. The difficulty of making magnetic interpretations on solutions of compounds which are strongly coupled (i.e., complexes such as **3** or protein cytochrome *c* oxidase samples) suggests that a more conservative lower limit of $-J$, i.e., $-J > \sim 50$ cm$^{-1}$ and not $-J > 200$ cm$^{-1}$, is realistic for the enzyme. The $^1$H-NMR spectrum of **3** is also consistent with substantial antiferromagnetic coupling since it gives a pyrrole signal shifted 15 ppm upfield from pure high-spin (F$_8$-TPP)Fe$^{III}$-L derivatives. In addition, there are several peaks in the +5 to −105 ppm region, tentatively assigned to the TMPA ligand; the emergence of these peaks is consistent with loss of pure $S = 1/2$ character on Cu(II) due to antiferromagnetic coupling and/or the effects of line narrowing due to enhanced electronic relaxation promoted by the proximal paramagnetic Fe(III).

Ongoing studies include the elucidation of the mechanism of formation of the title complex from $O_2$ chemistry, as well as the full physical characterization of the analogous $\mu$-hydroxo complex derived from protonation of **3**.[30]

**Acknowledgment.** This research is supported by the National Institutes of Health (GM28962, K.D.K.; GM 47295, B.H.H.; GM32394, E.P.D.) and the National Science Foundation (NSF DMB9001530, B.H.H.; CHE-9000471, Johns Hopkins University partial support for X-ray diffractometer purchase). For computations related to the magnetic studies, the Hewlett-Packard Apollo 9000/730 workstation was provided by the Cherry L. Emerson Center for Scientific Computation at Emory University.

**Supplementary Material Available:** Anisotropic thermal parameters and bond distances and angles for [(F$_8$-TPP)Fe$^{III}$-O-Cu$^{II}$(TMPA)](ClO$_4$)·3C$_7$H$_8$·2CH$_3$CN ((**3**-ClO$_4$)·3C$_7$H$_8$·2CH$_3$CN) and atomic coordinates, isotropic and anisotropic thermal parameters, and bond distances and bond angles for [(F$_8$-TPP)Fe]$_2$O·3C$_7$H$_8$ (20 pages); tables of observed and calculated structure factors (59 pages). This material is contained in many libraries on microfiche, immediately follows this article in the microfilm version of the journal, and can be ordered from the ACS; see any current masthead page for ordering information.